

# Physical properties and transmission spectrum of the WASP-80 planetary system from multi-colour photometry

L. Mancini<sup>1</sup>, J. Southworth<sup>2</sup>, S. Ciceri<sup>1</sup>, M. Dominik<sup>3</sup>, Th. Henning<sup>1</sup>, U. G. Jørgensen<sup>4,5</sup>, A. F. Lanza<sup>6</sup>, M. Rabus<sup>7,1</sup>, C. Snodgrass<sup>8</sup>, C. Vilela<sup>2</sup>, K. A. Alsubai<sup>9</sup>, V. Bozza<sup>10,11</sup>, D. M. Bramich<sup>12</sup>, S. Calchi Novati<sup>13,10</sup>, G. D'Ago<sup>10,11</sup>, R. Figuera Jaimes<sup>14,3</sup>, P. Galianni<sup>3</sup>, S.-H. Gu<sup>15,16</sup>, K. Harpsøe<sup>4,5</sup>, T. Hinse<sup>17</sup>, M. Hundertmark<sup>3</sup>, D. Juncher<sup>4,5</sup>, N. Kains<sup>14</sup>, H. Korhonen<sup>18,4,5</sup>, A. Popovas<sup>4,5</sup>, S. Rahvar<sup>19,20</sup>, J. Skottfelt<sup>4,5</sup>, R. Street<sup>21</sup>, J. Surdej<sup>22</sup>, Y. Tsapras<sup>21,23</sup>, X.-B. Wang<sup>15,16</sup>, and O. Wertz<sup>22</sup>

<sup>1</sup> Max Planck Institute for Astronomy, Königstuhl 17, 69117 – Heidelberg, Germany  
e-mail: [mancini@mpia.de](mailto:mancini@mpia.de)

<sup>2</sup> Astrophysics Group, Keele University, Staffordshire, ST5 5BG, UK

<sup>3</sup> SUPA, University of St Andrews, School of Physics & Astronomy, North Haugh, St Andrews, KY16 9SS, UK

<sup>4</sup> Niels Bohr Institute, University of Copenhagen, Juliane Maries vej 30, 2100 Copenhagen Ø, Denmark

<sup>5</sup> Centre for Star and Planet Formation, Geological Museum, Øster Voldgade 5-7, 1350 Copenhagen, Denmark

<sup>6</sup> INAF - Osservatorio Astrofisico di Catania, via S.Sofia 78, 95123 Catania, Italy

<sup>7</sup> Instituto de Astrofísica, Facultad de Física, Pontificia Universidad Católica de Chile, Av. Vicuña Mackenna 4860, 7820436 Macul, Santiago, Chile

<sup>8</sup> Max-Planck-Institute for Solar System Research, Max-Planck Str. 2, 37191 Katlenburg-Lindau, Germany

<sup>9</sup> Qatar Foundation, PO Box 5825, Doha, Qatar

<sup>10</sup> Dipartimento di Fisica “E.R. Caianiello”, University of Salerno, Via Giovanni Paolo II, 84084 Fisciano, Italy

<sup>11</sup> Istituto Nazionale di Fisica Nucleare, Sezione di Napoli, Napoli, Italy

<sup>12</sup> Qatar Environment and Energy Research Institute, Qatar Foundation, Tornado Tower, Floor 19, P.O. Box 5825, Doha, Qatar

<sup>13</sup> Istituto Internazionale per gli Alti Studi Scientifici (IIASS), 84019 Vietri Sul Mare (SA), Italy

<sup>14</sup> European Southern Observatory, Karl-Schwarzschild-Straße 2, 85748 Garching bei München, Germany

<sup>15</sup> Yunnan Observatory, Chinese Academy of Sciences, Kunming 650011, China

<sup>16</sup> Key Laboratory for the Structure and Evolution of Celestial Objects, Chinese Academy of Sciences, Kunming 650011, China

<sup>17</sup> Korea Astronomy and Space Science Institute, Daejeon 305-348, Republic of Korea

<sup>18</sup> Finnish Centre for Astronomy with ESO (FINCA), University of Turku, Väisäläntie 20, FI-21500 Piikkiö, Finland

<sup>19</sup> Department of Physics, Sharif University of Technology, P. O. Box 11155-9161 Tehran, Iran

<sup>20</sup> Perimeter Institute for Theoretical Physics, 31 Caroline St. N., Waterloo, ON, N2L 2Y5, Canada

<sup>21</sup> Las Cumbres Observatory Global Telescope Network, 6740B Cortona Drive, Goleta, CA 93117, USA

<sup>22</sup> Institut d'Astrophysique et de Géophysique, Université de Liège, 4000 Liège, Belgium

<sup>23</sup> School of Physics and Astronomy, Queen Mary University of London, Mile End Road, London, E1 4NS, UK

Preprint online version: September 15, 2021

## ABSTRACT

WASP-80 is one of only two systems known to contain a hot Jupiter which transits its M-dwarf host star. We present eight light curves of one transit event, obtained simultaneously using two defocussed telescopes. These data were taken through the Bessell  $I$ , Sloan  $g'r'i'z'$  and near-infrared  $JHK$  passbands. We use our data to search for opacity-induced changes in the planetary radius, but find that all values agree with each other. Our data are therefore consistent with a flat transmission spectrum to within the observational uncertainties. We also measure an activity index of the host star of  $\log R'_{\text{HK}} = -4.495$ , meaning that WASP-80 A shows strong chromospheric activity. The non-detection of starspots implies that, if they exist, they must be small and symmetrically distributed on the stellar surface. We model all available optical transit light curves and obtain improved physical properties and orbital ephemerides for the system.

**Key words.** stars: planetary systems – stars: fundamental parameters – stars: individual: WASP-80 – techniques: photometric

## 1. Introduction

Planetary systems in which the host star is a late-type dwarf are of particular interest because they have favourable ratios of planetary mass and radius to those of the star. This makes the detections of small and low-mass planets easier for the tran-

sit and Doppler methods, respectively. If the planet is transiting and the parent star is bright, then the planetary atmosphere can be probed by transmission spectroscopy (e.g. GJ 1214 b: Croll et al., 2011; Crossfield et al., 2011; Bean et al., 2011; Berta et al., 2012; Colón & Gaidos, 2013; GJ 3470 b: Crossfield et al., 2013; GJ 436 b: Pont et al., 2009; Gibson et al., 2011), trans-

**Table 2.** Excerpts of the light curves of WASP-80: this table will be made available at the CDS. A portion is shown here for guidance regarding its form and content.

Telescope	Filter	BJD (TDB)	Diff. mag.	Uncertainty
DK 1.54-m	<i>I</i>	2456459.732729	0.00002	0.00055
DK 1.54-m	<i>I</i>	2456459.733794	0.00029	0.00055
ESO 2.2-m	<i>g'</i>	2456459.708924	0.00122	0.00087
ESO 2.2-m	<i>g'</i>	2456459.710953	0.00079	0.00087
ESO 2.2-m	<i>r'</i>	2456459.715126	-0.00021	0.00033
ESO 2.2-m	<i>r'</i>	2456459.719854	0.00084	0.00033
ESO 2.2-m	<i>i'</i>	2456459.715126	0.00009	0.00064
ESO 2.2-m	<i>i'</i>	2456459.716988	-0.00059	0.00064
ESO 2.2-m	<i>z'</i>	2456459.715126	0.00041	0.00064
ESO 2.2-m	<i>z'</i>	2456459.719854	-0.00109	0.00064

mission photometry (e.g. GJ 1214 b: de Mooij et al., 2012; Murgas et al., 2012; de Mooij et al., 2013; Narita et al., 2013; GJ 3470 b: Nascimbeni et al., 2013) and observations of secondary eclipses (e.g. GJ 1214 b: Fraine et al., 2013; GJ 436 b: Stevenson et al., 2010; Knutson et al., 2011).

Recent analyses of HARPS and *Kepler* data suggest that Neptunes and super-Earths with orbital periods shorter than 50 days are very abundant around M stars (Bonfils et al., 2013; Dressing & Charbonneau, 2013). Bonfils et al. (2013) also established that giant planets have a much lower occurrence rate for orbital periods in the range 10–100 d, supporting the idea that the frequency of giant planets decreases toward less massive parent stars, irrespective of period (Johnson et al., 2010).

Accordingly, only two transiting hot Jupiters have so far been found orbiting M dwarfs<sup>1</sup>. These are Kepler-45 b (KOI-254;  $R_p = 0.999 R_{Jup}$ ,  $M_p = 0.500 M_{Jup}$ , Johnson et al., 2012; Southworth, 2012) and WASP-80 b ( $R_p = 0.95 R_{Jup}$ ,  $M_p = 0.55 M_{Jup}$ , Triaud et al., 2013). Whilst Kepler-45 is a distant (333 pc) and faint ( $V = 16.9$ ) star, WASP-80 is much closer (60 pc) and brighter ( $V = 11.9$ ), enabling a detailed study of its characteristics with ground-based facilities. Moreover, due to its low density and large transit depth ( $\sim 3\%$ ), WASP-80 b is a very suitable target for transmission spectroscopy and photometry.

Here we present photometric observations of a transit of WASP-80 b, observed simultaneously with two telescopes and in eight different passbands. We use these data to refine the physical parameters of the planetary system and provide the first probe of the day-night terminator region of this giant planet by transmission photometry.

## 2. Observations and data reduction

A complete transit of WASP-80 b was observed on 2013 June 16 (see Table 1), using the DFOSC imager mounted on the 1.54-m Danish Telescope at ESO La Silla during the 2013 observing campaign by the MiNDSTeP consortium (Dominik et al., 2010). The instrument has a field of view of  $13.7' \times 13.7'$  and a plate scale of  $0.39'' \text{ pixel}^{-1}$ . The observations were performed through a Bessel *I* filter and using the *defocussing* method. The telescope was autoguided and the CCD was windowed to reduce the readout time. The night was photometric.

<sup>1</sup> Two brown dwarfs are also known to transit M stars: NLTT 41135 (Irwin et al., 2010) and LHS 6343 (Johnson et al., 2011).

The data were reduced using DEFOT, an IDL<sup>2</sup> pipeline for time-series photometry (Southworth et al., 2009a). The images were debiased and flat-fielded using standard methods, then subjected to aperture photometry using the APER<sup>3</sup> task and an optimal ensemble of comparison stars. Pointing variations were followed by cross-correlating each image against a reference image. The shape of the light curve is very insensitive to the aperture sizes, so we chose those which yielded the lowest scatter. The final light curve was detrended to remove slow instrumental and astrophysical trends by fitting a straight line to the out-of-transit data. This process was simultaneous with the optimisation of the weights of an ensemble of comparison stars. The final differential-flux light curve is plotted in Fig. 1.

The same transit was also observed using the Gamma Ray Burst Optical and Near-Infrared Detector (GROND) instrument mounted on the MPG<sup>4</sup>/ESO 2.2-m telescope, also located at ESO La Silla. GROND is an imaging system capable of simultaneous photometric observations in four optical (similar to Sloan *g'*, *r'*, *i'*, *z'*) and three NIR (*J*, *H*, *K*) passbands (Greiner et al., 2008). Each of the four optical channels is equipped with a back-illuminated  $2048 \times 2048$  E2V CCD, with a field of view of  $5.4' \times 5.4'$  at  $0.158'' \text{ pixel}^{-1}$ . The three NIR channels use  $1024 \times 1024$  Rockwell HAWAII-1 arrays with a field of view of  $10' \times 10'$  at  $0.6'' \text{ pixel}^{-1}$ . The observations were also performed with the telescope defocussed.

The optical data were reduced as for the Danish Telescope, except that a quadratic function was used to detrend the light curves. The NIR data were reduced following the procedure described in Mancini et al. (2013c). The optical light curves are plotted superimposed in the bottom panel of Fig. 1 in order to highlight the differences among the transit depths and light curve shapes of the simultaneous multi-band observations. The GROND *i'* and Danish Telescope *I* light curves are in excellent agreement. The differential-magnitude light curves are given in Table 2.

### 2.1. Stellar activity measurement

We obtained a spectrum of the Ca II H and K lines on the night of 2012 October 1, using the William Herschel Telescope with the ISIS grating spectrograph, in order to measure the  $\log R'_{HK}$  stellar activity index. With the H2400B grating we obtained a spectrum covering 375–415 nm at a reciprocal dispersion of  $0.011 \text{ nm pixel}^{-1}$ . An exposure time of 600 s yielded a continuum signal to noise ratio of approximately 20 in the region of the H and K lines. The data were reduced using optimal extraction as implemented in the PAMELA and MOLLY packages (Marsh, 1989) and calibrated onto the Mt. Wilson system using 20 standard stars from Vaughan et al. (1978); further details can be found in Vilela et al. (in prep).

The very strong H and K emission lines for WASP-80 A (Fig. 2) yield the emission measure  $\log R'_{HK} = -4.495$ , which is indicative of high activity (e.g. Noyes et al., 1984). Given this strong chromospheric emission one might expect to see evidence of spot activity, but Triaud et al. (2013)

<sup>2</sup> IDL is a trademark of the ITT Visual Information Solutions: <http://www.itervis.com/ProductServices/IDL.aspx>

<sup>3</sup> APER is part of the ASTROLIB subroutine library distributed by NASA on <http://idlastro.gsfc.nasa.gov>.

<sup>4</sup> Max Planck Gesellschaft.

**Table 1.** Details of the transit observations presented in this work.  $N_{\text{obs}}$  is the number of observations,  $T_{\text{exp}}$  is the exposure time,  $T_{\text{obs}}$  is the observational cadence, and ‘Moon illum.’ is the fractional illumination of the Moon at the midpoint of the transit. The aperture sizes are the radii of the software apertures for the star, inner sky and outer sky, respectively. Scatter is the r.m.s. scatter of the data versus a fitted model.

Telescope	Date of first obs.	Start time (UT)	End time (UT)	$N_{\text{obs}}$	$T_{\text{exp}}$ (s)	$T_{\text{obs}}$ (s)	Filter	Airmass	Moon illum.	Aperture radii (px)	Scatter (mmag)
DFOSC	2013 06 16	05:35	09:44	200	60	75	Bessel $I$	1.33 → 1.12 → 1.37	46%	16, 38, 60	0.49
GROND	2013 06 16	05:00	10:50	162	60	120	Sloan $g'$	1.38 → 1.12 → 1.79	46%	30, 90, 120	0.80
GROND	2013 06 16	05:00	10:50	162	60	120	Sloan $r'$	1.38 → 1.12 → 1.79	46%	35, 100, 120	0.49
GROND	2013 06 16	05:00	10:50	162	60	120	Sloan $i'$	1.38 → 1.12 → 1.79	46%	35, 80, 100	0.82
GROND	2013 06 16	05:00	10:50	162	60	120	Sloan $z'$	1.38 → 1.12 → 1.79	46%	30, 80, 100	1.06
GROND	2013 06 16	05:00	10:50	523	4	38	$J$	1.38 → 1.12 → 1.79	46%	6, 11, 21	4.15
GROND	2013 06 16	05:00	10:50	523	4	38	$H$	1.38 → 1.12 → 1.79	46%	5, 12, 22	3.28
GROND	2013 06 16	05:00	10:50	523	4	38	$K$	1.38 → 1.12 → 1.79	46%	7, 11, 20	5.14

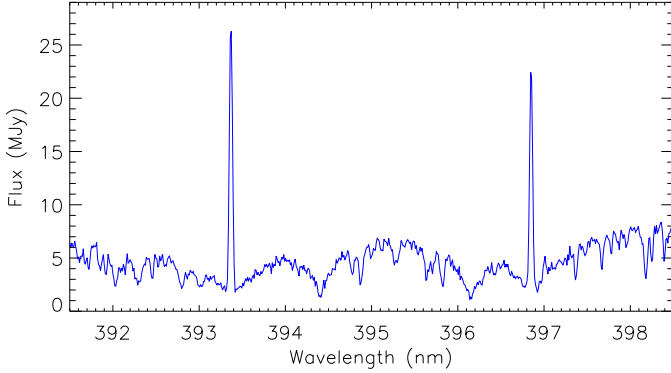


**Fig. 2.** Spectrum of WASP-80 in the region of the Ca II H and K lines showing the strong chromospheric emission in the line cores.

found no rotational modulation in the SuperWASP light curves to a limit of  $\sim 1$  mmag, and we see no evidence of spot anomalies (e.g. Tregloan-Reed et al., 2013) in our light curves. A plausible explanation is that the stellar surface contains many spots which are too small to noticeably affect transit light curves, and which are approximately symmetrically distributed so cause no measurable rotation signal in the SuperWASP light curves.

This suggestion is in agreement with the conclusions of Jackson & Jeffries (2012) (see also Jackson & Jeffries, 2013), who analysed two large samples of low-mass stars ( $0.2 < M_*/M_\odot < 0.7$ ) in the open cluster NGC 2516: one sample with measurable rotational modulation and one without. The two samples coincide on the colour-magnitude diagram for the cluster, and have the same rotational velocities and levels of chromospheric activity. This difference can be explained by the photometrically constant stars having many small starspots rather than few large ones.

In the case of WASP-80, assuming that the photometric modulation due to starspots is smaller than 1 mmag, we can estimate the maximum deviation of the covering factor from uniformity of a few  $10^{-3}$  of the disc area, by considering that the spot temperature contrast is probably smaller in cooler stars with respect to the Sun (see Berdyugina, 2005).

### 3. Light-curve analysis

The light curves were modelled using the JKTEBOP<sup>5</sup> code (see Southworth, 2012, and references therein), which represents the star and planet as biaxial spheroids for calculation of the reflection and ellipsoidal effects and as spheres for calculation of the eclipse shapes. The main parameters fitted by JKTEBOP are the orbital inclination,  $i$ , the transit midpoint,  $T_0$ , and the sum and ratio of the fractional radii of the star and planet,  $r_A + r_b$  and  $k = r_b/r_A$ . The fractional radii are defined as  $r_A = R_A/a$  and  $r_b = R_b/a$ , where  $a$  is the orbital semimajor axis, and  $R_A$  and  $R_b$  are the absolute radii of the star and the planet, respectively. Each light curve was modelled separately using the quadratic limb darkening (LD) law. The linear LD coefficients were fitted to the data whereas the quadratic LD coefficients were fixed at theoretical values (Claret, 2004b) but perturbed by  $\pm 0.1$  during the process of error estimation. We assumed that the orbit was circular (Triaud et al., 2013). We included in the fits the coefficients of a linear (DFOSC) or quadratic (GROND) polynomial versus time in order to fully account for the uncertainty in the detrending of the light curves.

Time-series photometry is unavoidably afflicted by correlated (red) noise which is not accounted for by standard error estimation algorithms (e.g. Carter & Winn, 2009). The APER algorithm we use to perform aperture photometry also tends to underestimate the true uncertainties in the relative magnitude measurements. We therefore rescaled the errorbars as in our previous works (Mancini et al., 2013a,b,c), first to give a reduced  $\chi^2$  of  $\chi_\nu^2 = 1$  and then using the  $\beta$  approach (e.g. Gillon et al., 2006; Winn et al., 2008; Gibson et al., 2008).

#### 3.1. Orbital period determination

We used our photometric data to refine the orbital period of WASP-80 b. The transit time for each of our datasets was obtained by fitting with JKTEBOP, and uncertainties were estimated using Monte Carlo simulations. We also modelled the follow-up light curves reported in Triaud et al. (2013) in order to obtain a timing for each dataset. All timings were placed on the BJD(TDB) time system and are summarised in Table 3. The resulting measurements of transit midpoints were fitted with a straight line to obtain a final orbital ephemeris:

$$T_0 = \text{BJD(TDB)} 2\,456\,125.417405(99) + 3.06786144(87) E,$$

<sup>5</sup> The source code of JKTEBOP is available at: <http://www.astro.keele.ac.uk/jkt/codes/jktebop.html>

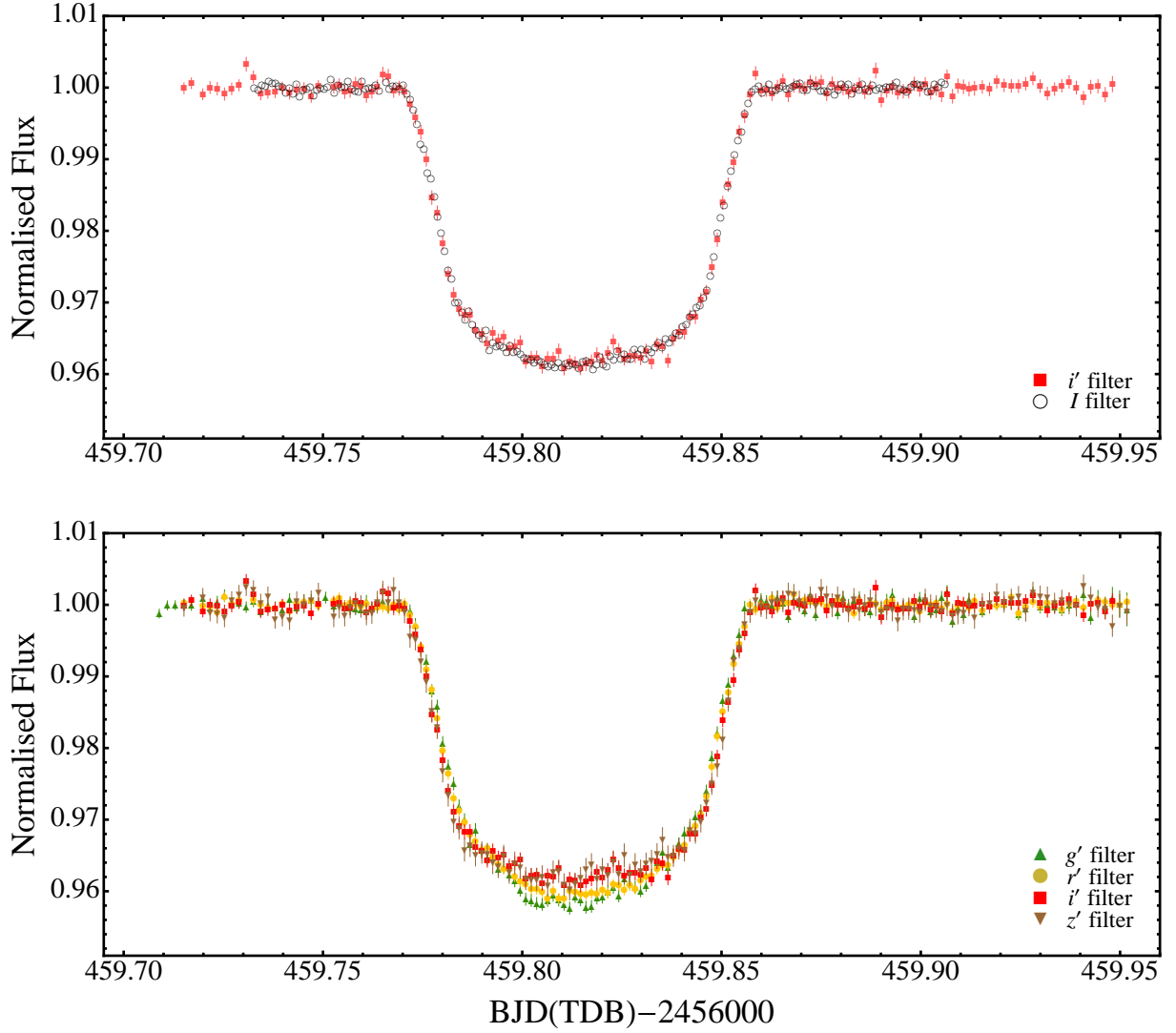


**Fig. 1.** Light curves of a transit of WASP-80 b. *Top panel:* light curves obtained with the Danish Telescope (Bessel-*I* filter) and with GROND (Sloan-*i'*), highlighting the good match between the transit shapes in the two independent observations. The circles denoting the DK points have the same size of the corresponding error bars, which have been suppressed for clarity. *Bottom panel:* light curves obtained with GROND through four optical filters simultaneously, showing how the transit shape changes with wavelength.

**Table 3.** Times of mid-transit of WASP-80 b and their residuals versus a linear orbital ephemeris.

Time of minimum BJD(TDB)–2400000	Cycle no.	Residual (d)	Reference
56054.856812 ± 0.000135	-23	0.000220	1
56134.620911 ± 0.000222	3	-0.000078	1
56180.638678 ± 0.000165	18	-0.000233	1
56459.814384 ± 0.000044	109	0.000081	2
56459.814284 ± 0.000096	109	-0.000019	3
56459.814414 ± 0.000082	109	0.000111	4
56459.814350 ± 0.000103	109	0.000047	5
56459.814233 ± 0.000161	109	-0.000070	6

**Notes.** References: (1) Triaud et al. (2013); (2) Danish telescope (this work); (3) GROND *g'* (this work); (4) GROND *r'* (this work); (5) GROND *i'* (this work); (6) GROND *z'* (this work).

where  $E$  is the number of orbital cycles after the reference epoch, which we take to be that estimated by Triaud et al.

(2013), and quantities in brackets denote the uncertainty in the final digit of the preceding number. The quality of fit,  $\chi^2_\nu = 0.99$ , indicates that a linear ephemeris is a good match to the observations. A plot of the residuals (Fig. 3) shows no evidence for systematic deviations from the predicted transit times. However, the number of observed transits of this planet is still very low so transit timing variations cannot be ruled out.

### 3.2. Photometric parameters

The GROND light curves and the JKTEBOP best-fitting models are shown in Fig. 4. A similar plot is reported in Fig. 5 for the light curves from the Danish Telescope and from Triaud et al. (2013). The parameters of the fits are given in Table 4. Uncertainties in the fitted parameters from each solution were calculated from 3500 Monte Carlo simulations and by a residual-permutation algorithm (Southworth, 2008). The larger of the two possible error

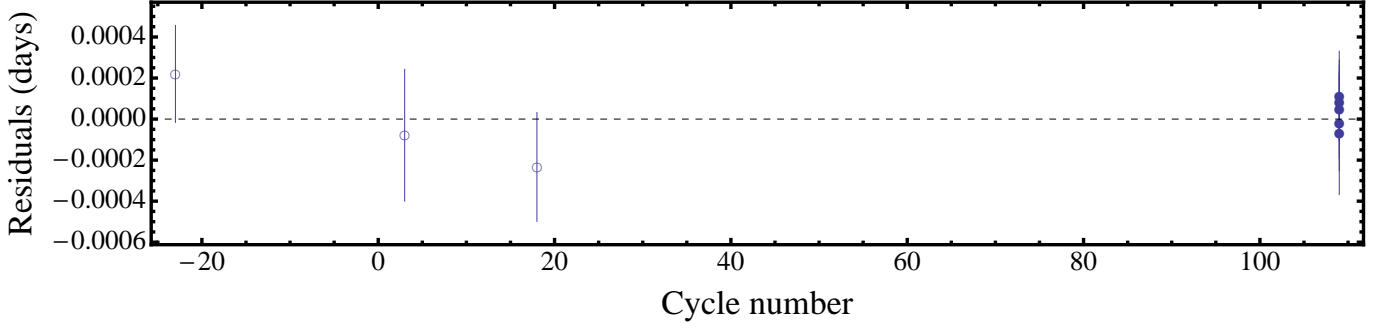


**Fig. 3.** Plot of the residuals of the timings of mid-transit of WASP-80 b versus a linear ephemeris. Timings based on the observations obtained by Triaud et al. (2013) are plotted using open circles, while the other timings (this work) are plotted with filled circles.

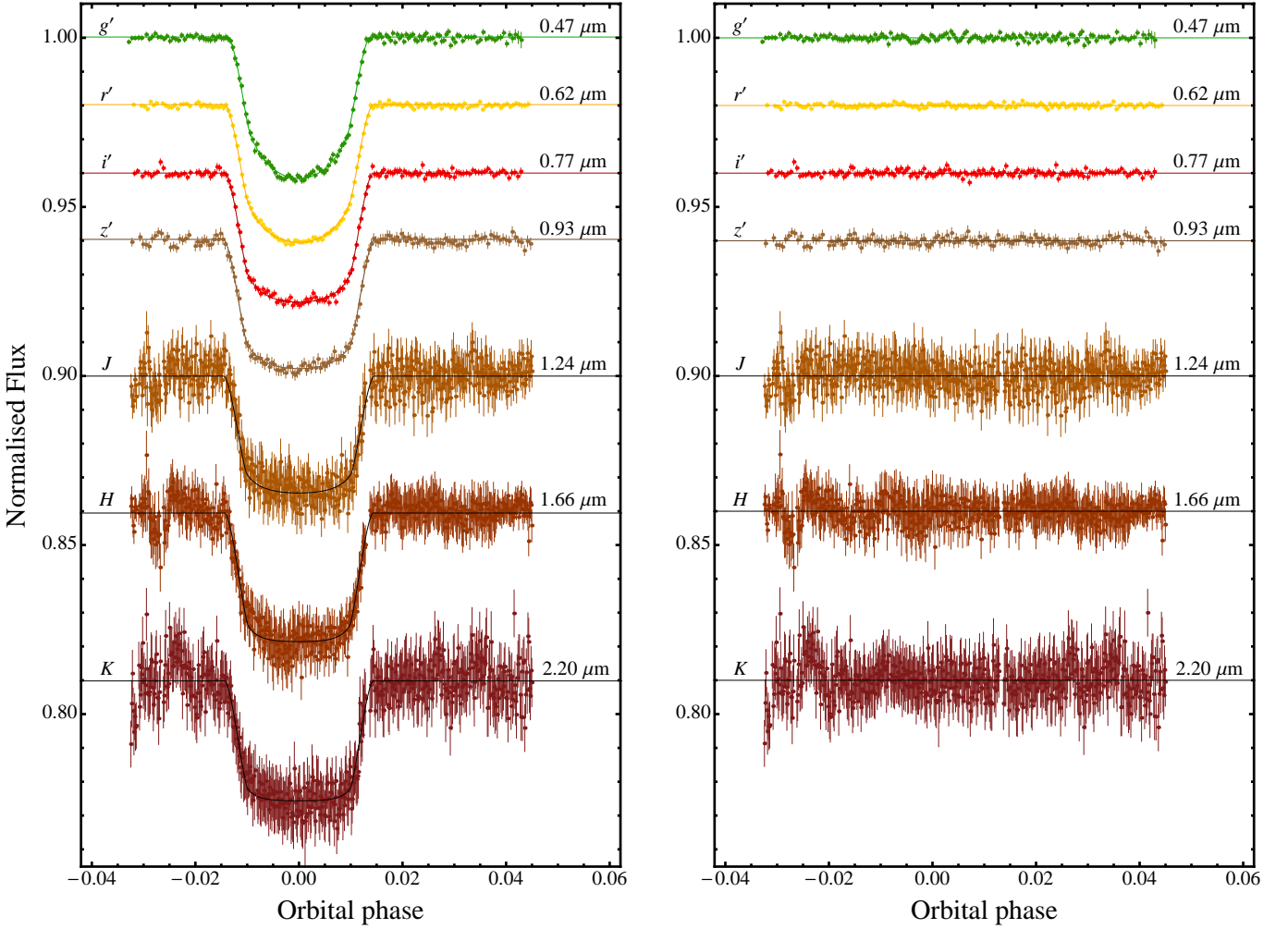


**Fig. 4.** *Left-hand panel:* simultaneous optical and NIR light curves of the transit event of WASP-80 b observed with GROND. The JKTEBOP best fits are shown as solid lines for each optical data set. The passbands are labelled on the left of the figure, and their central wavelengths are given on the right. *Right-hand panel:* the residuals of each fit.

bars was retained in each case. The final photometric parameters are the weighted mean of the results presented in Table 4. Values obtained by Triaud et al. (2013) are also reported for comparison. Due to their lower quality (see Fig. 4), we did not use the GROND-NIR light curves to estimate the final photometric parameters of WASP-80.

#### 4. Physical properties

Following the *Homogeneous Studies* approach (Southworth, 2012, and references therein), we used the photometric parameters estimated in the previous section and the spectroscopic properties of the parent star (velocity amplitude  $K_A = 110.9^{+3.0}_{-3.3} \text{ ms}^{-1}$ , effective temperature  $T_{\text{eff}} = 4145 \pm 100 \text{ K}$  and metallicity  $[\frac{\text{Fe}}{\text{H}}] = -0.14 \pm 0.16$ ) taken

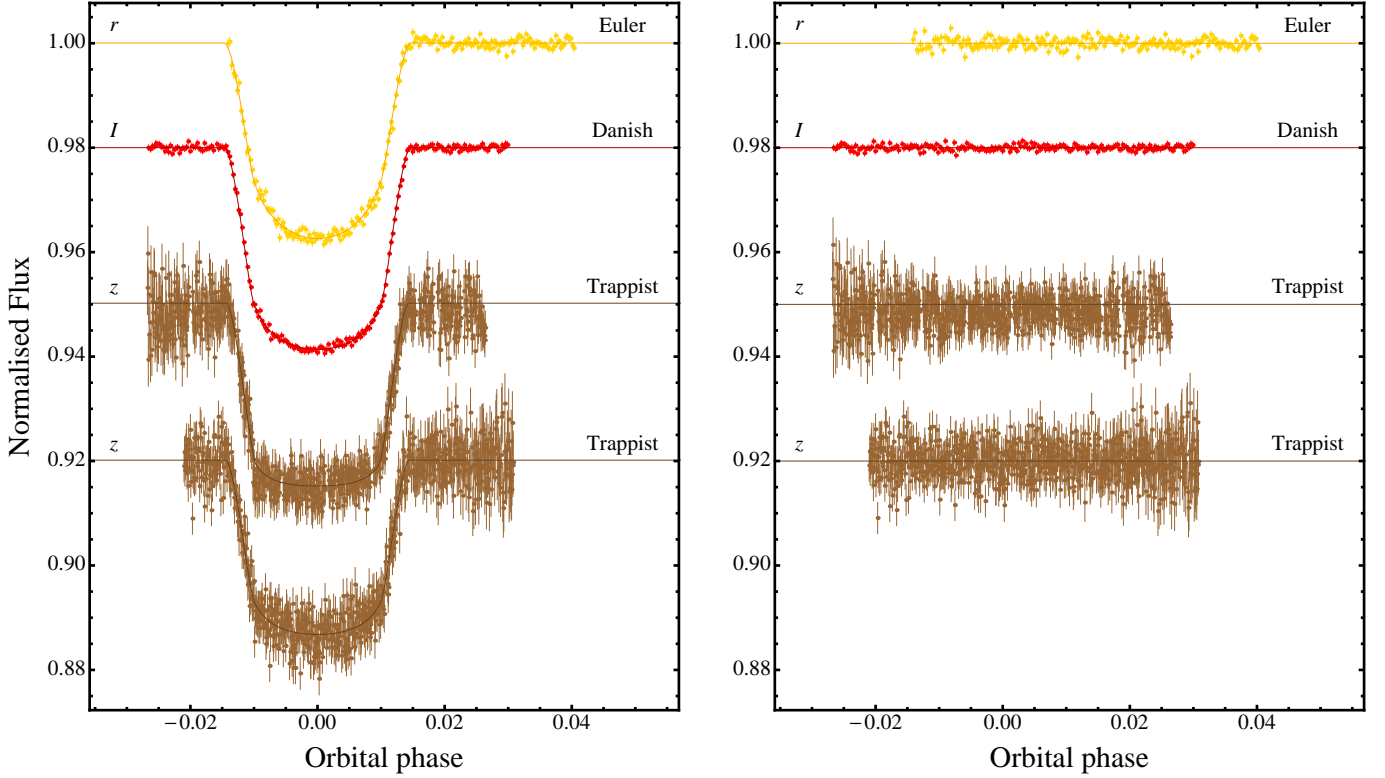


**Fig. 5.** *Left-hand panel:* Light curves of transit events of WASP-80 b observed in Gunn  $r$  with the Euler telescope (Triaud et al., 2013), in Bessel  $I$  with the Danish telescope (this work) and in  $z$  with TRAPPIST (Triaud et al., 2013). The light curves are ordered according to central wavelength of the filter used. The JKTEBOP best fits are shown as solid lines for each optical data set. *Right-hand panel:* the residuals of each fit.

**Table 4.** Parameters of the JKTEBOP fits to the light curves of WASP-80. The final parameters, given in bold, are the weighted means of the results for the datasets. Results from the discovery paper are included at the base of the table for comparison.

Telescope	Filter	$r_A + r_b$	$k$	$i^\circ$	$r_A$	$r_b$
Danish 1.54-m	Bessel $I$	$0.09324 \pm 0.00095$	$0.17135 \pm 0.00099$	$88.99 \pm 0.23$	$0.07960 \pm 0.00074$	$0.01364 \pm 0.00018$
MPG/ESO 2.2-m	Sloan $g'$	$0.09131 \pm 0.00161$	$0.17033 \pm 0.00217$	$89.20 \pm 0.59$	$0.07802 \pm 0.00128$	$0.01329 \pm 0.00035$
MPG/ESO 2.2-m	Sloan $r'$	$0.09001 \pm 0.00290$	$0.17041 \pm 0.00175$	$89.16 \pm 0.50$	$0.07691 \pm 0.00245$	$0.01311 \pm 0.00047$
MPG/ESO 2.2-m	Sloan $i'$	$0.09239 \pm 0.00167$	$0.17183 \pm 0.00161$	$89.10 \pm 0.58$	$0.07885 \pm 0.00134$	$0.01355 \pm 0.00033$
MPG/ESO 2.2-m	Sloan $z'$	$0.09391 \pm 0.00575$	$0.17274 \pm 0.00226$	$89.11 \pm 0.72$	$0.08007 \pm 0.00091$	$0.01383 \pm 0.00090$
MPG/ESO 2.2-m	$J$	$0.08937 \pm 0.00567$	$0.16813 \pm 0.00424$	$90.00 \pm 1.16$	$0.07651 \pm 0.00476$	$0.01286 \pm 0.00094$
MPG/ESO 2.2-m	$H$	$0.09393 \pm 0.00365$	$0.17525 \pm 0.00472$	$89.34 \pm 0.91$	$0.07993 \pm 0.00296$	$0.01401 \pm 0.00076$
MPG/ESO 2.2-m	$K$	$0.09067 \pm 0.00773$	$0.16383 \pm 0.00809$	$89.99 \pm 1.29$	$0.07791 \pm 0.00673$	$0.01276 \pm 0.00128$
Euler 1.2-m	Gunn $r$	$0.09694 \pm 0.00277$	$0.16726 \pm 0.00270$	$88.43 \pm 0.45$	$0.08305 \pm 0.00223$	$0.01389 \pm 0.00059$
Trappist 0.60-m	Gunn $z$	$0.09261 \pm 0.00251$	$0.17079 \pm 0.00201$	$88.64 \pm 0.49$	$0.07910 \pm 0.00204$	$0.01351 \pm 0.00047$
Trappist 0.60-m	Gunn $z$	$0.09464 \pm 0.00550$	$0.16285 \pm 0.00230$	$88.63 \pm 0.87$	$0.08139 \pm 0.00467$	$0.01325 \pm 0.00087$
<b>Final results</b>		<b><math>0.09283 \pm 0.00058</math></b>	<b><math>0.17058 \pm 0.00057</math></b>	<b><math>88.91 \pm 0.16</math></b>	<b><math>0.07929 \pm 0.00046</math></b>	<b><math>0.01354 \pm 0.00012</math></b>
Triaud et al. (2013)		—	$0.17126^{+0.00031}_{-0.00026}$	$89.92^{+0.07}_{-0.12}$	—	—

from Triaud et al. (2013), to revise the physical properties of the WASP-80 system using the ABSDIM code.

We iteratively determined the velocity amplitude of the planet ( $K_b$ ) which yielded the best agreement between the measured  $R_A/a$  and  $T_{\text{eff}}$ , and those predicted by a set of theoretical stellar models for the calculated stellar mass and  $[\frac{\text{Fe}}{\text{H}}]$ . The overall best fit was found over a grid of ages extending from the zero-age main sequence to a maximum of 5 Gyr, imposed because WASP-80 A shows strong activity indicative of youth (e.g. West et al., 2008). Statistical errors were propagated by a perturbation analysis. Systematic errors were estimated by calculating sets of results using five different sets of theoretical models

(Claret, 2004a; Demarque et al., 2004; Pietrinferni et al., 2004; VandenBerg et al., 2006; Dotter et al., 2008). The five models were given equal relative weighting. The resulting estimates of the physical properties are given in Table 5. For completeness we also estimated the physical properties of the WASP-80 system using empirical calibrations based on detached eclipsing binary systems, instead of theoretical stellar models, using the method proposed by Enoch et al. (2010) and the calibration equations by Southworth (2010). Table 5 shows that the system properties obtained using the empirical calibration and the theoretical model sets agree well, except for the models by Claret (2004a). This discrepancy can be attributed to the differences in the  $T_{\text{eff}}$



scale predicted by the various model sets (see Fig. 4 in Southworth, 2010).

Theoretical models prefer a larger age for the system than is reasonable based on the activity level of the host star. There are several cases (e.g. CoRoT-2 and HD 189733), where a planet-hosting star displays a much higher magnetic activity level than expected for their age (Poppenhaeger & Wolk, 2013). A similar behaviour has also been suggested in the case of Qatar-1 (Covino et al., 2013). Several studies pointed out that a close-in hot-Jupiter can produce different effects on its parent star. Tidal forces can increase the rotational velocity of the star (Pont, 2009). The effect of the magnetized stellar wind, which causes loss of angular momentum, is inhibited by the planet (Lanza et al., 2010; Cohen et al., 2010). Both processes make the star appear younger than it is. This situation can be investigated through a detailed spectroscopic analysis of the host star to refine its measured atmospheric parameters, and a study of its X-ray luminosity, which is known to decline with stellar age (e.g. Wright et al., 2011). In the meantime we do not report an age measurement for the system.

For the final system properties we took the unweighted means of the four concordant model sets and calculated systematic errorbars based on the interagreement between them. A comparison between our final values and those found by Triaud et al. (2013) is given in Table 6.

## 5. Variation of the planetary radius with wavelength

WASP-80 b is a good target for studies of the planetary atmosphere due to the low surface gravity, deep transit, and bright host star. However, its moderate equilibrium temperature ( $T_{\text{eq}}' = 825 \pm 20$  K) indicates that the planet should belong to the pL class, as suggested by Fortney et al. (2008). We therefore do not expect a big variation of the measured planet radius with wavelength. Our GROND data, however, are very well suited to investigating this possibility as they cover many passbands.

We have measured the ratio of the planetary and stellar radius,  $k$ , in the GROND light curves. Fig. 6 shows the result as a function of wavelength. The vertical errorbars represent the relative errors in the measurements (i.e. neglecting sources of error which affect all light curves equally), and the horizontal errorbars show the FWHM transmission of the passbands used. Due to the very large uncertainty, the values of  $k$  measured in the  $H$  and  $K$  bands were ignored. For the  $J$  band, following Southworth et al. (2012) and Mancini et al. (2013b), we refitted the data with all parameters fixed to the final values given in Table 4, with the exception of  $k$ . This approach maximizes the precision of estimations of the planet/star radius ratio. As our final value for  $k$  in the  $J$  band, we got  $k = 0.1695 \pm 0.0028$ .

The  $k$  found for the data from the Danish Telescope is also shown in green, and is a good match with the results for the GROND  $i'$  data. For illustration, Fig. 6 also shows the predictions from a model atmosphere calculated by Fortney et al. (2010) for a Jupiter-mass planet with gravity  $g_b = 10 \text{ m s}^{-2}$ , a base radius of  $1.25 R_{\text{Jup}}$  at 10 bar, and  $T_{\text{eq}}' = 750$  K. The opacity of strong-absorber molecules, such as gaseous titanium oxide (TiO) and vanadium oxide (VO), was removed from the model. Our experimental

points are in agreement with the prominent absorption features of the model and, being compatible with a flat transmission spectrum, do not indicate any large variation of the WASP-80 b's radius.

## 6. Summary and conclusions

The WASP-80 system contains a low-mass star which is at the border of the M spectral class, and a transiting hot Jupiter. It is one of only two systems containing an M-dwarf and a Jupiter-size object, the other being the much fainter Kepler-45. The brightness and small radius of the host star, which means the planetary transits are deep, and the low surface gravity of the planet make it a very important object for studying the atmospheric characteristics of irradiated gas giant planets.

We present eight light curves of one transit event, taken simultaneously using two telescopes, in the Bessell  $I$ , Sloan  $g'$ ,  $r'$ ,  $i'$ ,  $z'$ , and the near-IR  $JHK$  passbands. We find a good agreement for the ratio of the planetary to stellar radius determined from our optical light curves, which means that we do not detect any opacity-induced changes in planetary radius. We model all available optical transit light curves and use these results to determine the physical properties of the system. Our values are consistent with previous measurements, although our value for the planetary radius is  $1\sigma$  larger than that in the discovery paper.

We also present a spectrum of WASP-80 covering the Ca H and K lines, which shows strong emission in the line cores. We measure a chromospheric activity indicator of  $\log R'_{\text{HK}} = -4.495$ , which makes WASP-80 one of the most active planet hosts known. This implies strong magnetic activity and the presence of starspots, although we see no evidence in our high-precision photometry for starspot crossing events. If starspots exist on the surface of WASP-80 A, they are likely small, numerous and evenly distributed on the stellar photosphere.

Triaud et al. (2013) do not report a conclusive measurement of  $v \sin i_*$ . This is because the one obtained by the broadening of the spectral lines is incompatible with the one derived from fitting the Rossiter-McLaughlin effect, suggesting that the planet's orbital spin could be very inclined. Since the stellar rotation period is highly uncertain, an estimate of the stellar age based on gyrochronology is not possible. The age constraints implied by the stellar models in Sect. 4 are older than the strong activity of WASP-80 A suggests (see Pace, 2013, Fig. 1). A possible explanation is that the stellar activity is enhanced by its planet. However, an estimation of the stellar age based on theoretical models is very uncertain because M stars evolve very slowly during their main-sequence lifetime. X-ray observations may help explain this discrepancy.

A detailed characterisation of the atmosphere of WASP-80 b could be performed using transmission spectroscopy. We caution that such investigations should be based on simultaneous observations in order to avoid complications due to starspot activity.

**Acknowledgements.** This paper is based on observations collected with the MPG/ESO 2.2-m and the Danish 1.54-m telescopes, both located at ESO La Silla, Chile. Operation of the MPG/ESO 2.2-m telescope is jointly performed by the Max Planck Gesellschaft and the European Southern Observatory. Operation of the Danish telescope is based on a grant to U.G.J. by the Danish Natural Science Research Council (FNU). GROND was built by the high-energy group of MPE in collaboration with the LSW Tautenburg

**Table 5.** Derived physical properties of the WASP-80 planetary system using empirical calibrations and each of five sets of theoretical models.

	This work (dEB constraint)	This work (Claret models)	This work (Y <sup>2</sup> models)	This work (Teramo models)	This work (VRSS models)	This work (DSEP models)
$K_b$ (km s <sup>-1</sup> )	122.7 ± 2.8	126.9 ± 1.3	122.7 ± 2.3	122.5 ± 2.2	124.2 ± 1.7	123.6 ± 1.8
$M_A$ ( $M_\odot$ )	0.589 ± 0.040	0.652 ± 0.020	0.588 ± 0.034	0.585 ± 0.032	0.610 ± 0.024	0.602 ± 0.026
$R_A$ ( $R_\odot$ )	0.590 ± 0.014	0.611 ± 0.007	0.590 ± 0.014	0.589 ± 0.011	0.597 ± 0.009	0.595 ± 0.010
log $g_A$ (cgs)	4.666 ± 0.011	4.681 ± 0.007	4.666 ± 0.006	4.665 ± 0.009	4.671 ± 0.008	4.669 ± 0.008
$M_b$ ( $M_{Jup}$ )	0.557 ± 0.030	0.596 ± 0.020	0.557 ± 0.030	0.555 ± 0.025	0.571 ± 0.022	0.566 ± 0.023
$R_b$ ( $R_{Jup}$ )	0.981 ± 0.024	1.015 ± 0.014	0.981 ± 0.023	0.979 ± 0.020	0.993 ± 0.016	0.989 ± 0.017
$\rho_b$ ( $\rho_{Jup}$ )	0.551 ± 0.024	0.533 ± 0.021	0.551 ± 0.025	0.552 ± 0.023	0.545 ± 0.022	0.547 ± 0.022
$\Theta$	0.0668 ± 0.0024	0.0645 ± 0.0020	0.0668 ± 0.0025	0.0669 ± 0.0023	0.0660 ± 0.0021	0.0663 ± 0.0021
$a$ (AU)	0.03464 ± 0.00079	0.03583 ± 0.00037	0.03463 ± 0.00064	0.03457 ± 0.00062	0.03506 ± 0.00047	0.03490 ± 0.00050

**Table 6.** Final physical properties of the WASP-80 planetary system, compared with results from Triaud et al. (2013). Separate statistical and systematic error bars are given for the results from the current work.

		This work (final)	Triaud et al. (2013)
Stellar mass	$M_A$ ( $M_\odot$ )	0.596 ± 0.032 ± 0.014	0.57 <sup>+0.05</sup> <sub>-0.05</sub>
Stellar radius	$R_A$ ( $R_\odot$ )	0.593 ± 0.011 ± 0.005	0.571 <sup>+0.016</sup> <sub>-0.016</sub>
Stellar surface gravity	log $g_A$ (cgs)	4.6678 ± 0.0077 ± 0.0034	4.689 <sup>+0.012</sup> <sub>-0.013</sub>
Stellar density	$\rho_A$ ( $\rho_\odot$ )	2.862 ± 0.050	3.117 <sup>+0.021</sup> <sub>-0.020</sub>
Planetary mass	$M_b$ ( $M_{Jup}$ )	0.562 ± 0.025 ± 0.009	0.554 <sup>+0.030</sup> <sub>-0.039</sub>
Planetary radius	$R_b$ ( $R_{Jup}$ )	0.986 ± 0.020 ± 0.008	0.952 <sup>+0.026</sup> <sub>-0.027</sub>
Planetary surface gravity	$g_b$ (m s <sup>-2</sup> )	14.34 ± 0.46	15.07 <sup>+0.45</sup> <sub>-0.42</sub>
Planetary density	$\rho_b$ ( $\rho_{Jup}$ )	0.549 ± 0.023 ± 0.004	0.554 <sup>+0.030</sup> <sub>-0.039</sub>
Planetary equilibrium temperature	$T'_{eq}$ (K)	825 ± 20	~ 800
Safronov number	$\Theta$	0.0665 ± 0.0023 ± 0.0005	–
Orbital semimajor axis	$a$ (au)	0.03479 ± 0.00062 ± 0.00027	0.0346 <sup>+0.008</sup> <sub>-0.011</sub>

and ESO, and is operated as a PI-instrument at the MPG/ESO 2.2-m telescope. J.S. (Keele) acknowledges financial support from STFC in the form of an Advanced Fellowship. C.S. received funding from the European Union Seventh Framework Programme (FP7/2007-2013) under grant agreement no. 268421. M.R. acknowledges support from FONDECYT postdoctoral fellowship N°3120097. S.-H.G. and X.-B.W. would like to thank the financial support from National Natural Science Foundation of China (No.10873031) and Chinese Academy of Sciences (project KJCX2-YW-T24). O.W. thanks the Belgian National Fund for Scientific Research (FNRS). J.S. and O.W. acknowledge support from the Communauté française de Belgique – Action de recherche concertées – Académie universitaire Wallonie-Europe. K.A., M.D. and M.H. acknowledge grant NPRP-09-476-1-78 from the Qatar National Research Fund (a member of Qatar Foundation). The reduced light curves presented in this work will be made available at the CDS (<http://cdsweb.u-strasbg.fr/>). The following internet-based resources were used in research for this paper: the ESO Digitized Sky Survey; the NASA Astrophysics Data System; the SIMBAD data base operated at CDS, Strasbourg, France; and the arXiv scientific paper preprint service operated by Cornell University.

## References

- Bean, J. L., Désert, J.-M., Kabath, P., et al. 2011, *ApJ*, 743, 92  
 Berdyugina, S. V. 2005, *LRSP*, 2, 8  
 Berta, Z. K., Charbonneau, D., Désert, J.-M., et al. 2012, *ApJ*, 747, 35  
 Bonfils, X., Delfosse, X., Udry, S., et al. 2013, 549, A109  
 Carter, J. A., & Winn, J. N., 2009, *ApJ*, 704, 51  
 Claret, A. 2004, *A&A*, 424, 919  
 Claret, A. 2004, *A&A*, 428, 1001  
 Cohen, O., Drake, J. J., Kashyap, V. L., et al. 2010, *ApJ*, 723, L64  
 Colón, K. D., & Gaidos, E. 2013, *ApJ*, 776, 49  
 Covino, E., Esposito, M., Barbieri, M., et al. 2013, *A&A*, 554, A28  
 Croll, B., Albert, L., Jayawardhana, R., et al., 2011, *ApJ*, 736, 78  
 Crossfield, I. J. M., Barman, T., Hansen, B. M. S. 2011, *ApJ*, 736, 132  
 Crossfield, I. J. M., Barman, T., Hansen, B. M. S., Howard, A. 2013, *A&A*, 559, A33  
 de Mooij, E. J. W., Brogi, M., de Kok, R. J., et al. 2012, *A&A*, 538, A46  
 Demarque, P., Woo, J.-H., Kim, Y.-C., Yi, S. K., 2004, *ApJS*, 155, 667  
 de Mooij, E. J. W., Brogi, M., de Kok, R. J., et al. 2013, *ApJ*, 771, 109  
 Dominik, M., Jørgensen, U. G., Rattenbury, N. J., et al. 2010, *AN*, 331, 671  
 Dotter, A., Chaboyer, B., Jevremović, D., Kostov, V., Baron, E., Ferguson, J. W., 2008, *ApJS*, 178, 89  
 Dressing, C. D., & Charbonneau, D. 2013, *ApJ*, 767, 95  
 Enoch, B., Collier Cameron, A., Parley, N. R., Hebb, L., 2010, *A&A*, 516, A33  
 Fortney, J. J., Lodders, K., Marley, M. S., Freedman R. S., 2008, *ApJ*, 678, 1419  
 Fortney, J. J., Shabram, M., Showman, A. P., 2010, *ApJ*, 709, 1396  
 Fraine, J. D., Deming, D., Gillon, M., et al. 2013, *ApJ*, 765, 127  
 Gibson, N. P., Pollacco D., Simpson E. K., et al. 2008, *A&A*, 492, 603  
 Gibson, N. P., Pont, F., Aigrain, S. 2011, *MNRAS*, 411, 2199  
 Gillon, M., Pont, F., Moutou, C., et al. 2006, *A&A*, 459, 249  
 Greiner, J., Bornemann, W., Clemens, C., et al. 2008, *PASP*, 120, 405  
 Irwin, J., Buchhave, L., Berta, Z. K., et al. 2010, *ApJ*, 718, 1353  
 Jackson, R. J. & Jeffries, R. D. 2012, *MNRAS*, 423, 2966  
 Jackson, R. J. & Jeffries, R. D. 2013, *MNRAS*, 431, 1883  
 Johnson, J. A., Aller, K. M., Howard, A. W., Crepp, J. R. 2010, *PASP*, 122, 905  
 Johnson, J. A., Apps, K., Gazak, J. Z., et al. 2011, *ApJ*, 730, 79  
 Johnson, J. A., Gazak, J. Z., Apps, K., et al. 2012, *AJ*, 143, 111  
 Knutson, H. A., Madhusudhan, N., Cowan, N. B., et al. 2011, *ApJ*, 735, 27  
 Lanza, A. F. 2010, *A&A*, 512, A77  
 Mancini, L., Southworth, J., Ciceri, S., et al. 2013a, *A&A*, 551, A11  
 Mancini, L., Nikolov, N., Southworth, J., et al. 2013b, *MNRAS*, 430, 2932  
 Mancini, L., Ciceri, S., Chen, G., et al. 2013c, *MNRAS*, 436, 2  
 Marsh, T. R., 1989, *PASP*, 101, 1032  
 Murgas, F., Pallé, E., Cabrera-Lavers, A., et al. 2012, *A&A*, 544, A41



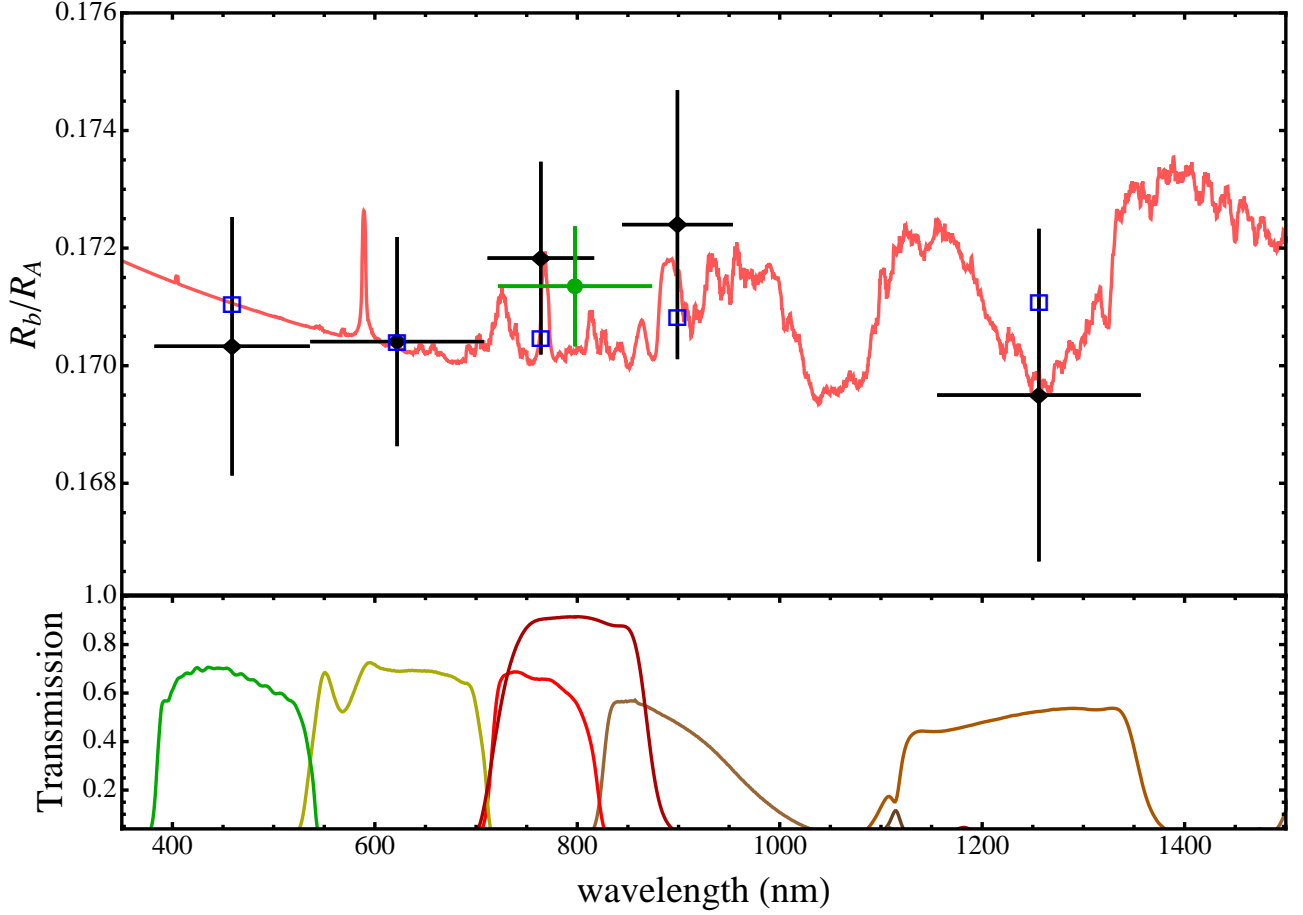


**Fig. 6.** Variation of the planetary radius, in terms of planet/star radius ratio, with wavelength. The black diamonds are from the transit observations performed with GROND while the green point is from the same transit observed using the Danish Telescope. The vertical bars represent the errors in the measurements and the horizontal bars show the FWHM transmission of the passbands used. The observational points are compared with a synthetic spectrum (see text for details). Transmission curves for the Bessel *I* filter and the total efficiencies of the GROND filters are shown in the bottom panel. The blue boxes indicate the predicted values for the model integrated over the passbands of the observations.

Narita, N., Fukui, A., Ikoma, M., et al. 2013, *ApJ*, 773, 144  
 Nascimbeni, V., Cunial, A., Murabito, S., et al. 2013, *A&A*, 549, A30  
 Noyes, R. W., Hartmann, L. W., Baliunas, et al. 1984, *ApJ*, 279, 763  
 Pace, G. 2013, *A&A*, 551, L8  
 Pietrinferni, A., Cassisi, S., Salaris, M., Castelli, F., 2004, *ApJ*, 612, 168  
 Pont, F. 2009, *MNRAS*, 396, 1789  
 Pont, F., Gilliland, R. L., Knutson, H., et al. 2009, *MNRAS*, 393, L6  
 Poppenhaeager, K., Wolk, S. J. 2013, to be published in the Proceedings of IAUS 302: Magnetic Fields Throughout Stellar Evolution, arXiv:1309.6356  
 Southworth, J. 2008, *MNRAS*, 386, 1644  
 Southworth, J. 2009, *MNRAS*, 394, 272  
 Southworth, J. 2010, *MNRAS*, 408, 1689  
 Southworth, J. 2012, *MNRAS*, 426, 1291  
 Southworth, J., Hinse, T. C., Jørgensen, U. G., et al. 2009a, *MNRAS*, 396, 1023  
 Stevenson, K. B., Harrington, J., Nymeyer, S., et al. 2010, *Nature*, 464, 161

Southworth, J., Mancini, L., Maxted, P. F. L., et al. 2012, *MNRAS*, 422, 3099  
 Tregloan-Reed, J., Southworth, J., Tappert, C. 2013, *MNRAS*, 428, 3671  
 Triaud, A. H. M. J., Anderson, D. R., Collier Cameron, A., et al. 2013, *A&A*, 551, A80  
 VandenBerg, D. A., Bergbusch, P. A., Dowler, P. D., 2006, *ApJS*, 162, 375  
 Vaughan, A. H., Preston, G. W., Wilson, O. C. 1978, *PASP*, 90, 267  
 West, A. A., Hawley, S. L., Bochanski, J. J. 2008, *ApJ*, 135, 785  
 Winn, J. N., Holman, M. J., Torres, G., et al. 2008, *ApJ*, 683, 1076  
 Wright, N. J., Drake, J. J., Mamajek, E. E., Henry, G. W. 2011, *ApJ*, 743, 48